Optimization of the short-circuit current in an InP nanowire array solar cell through opto-electronic modeling

Chen, Yang; Kivisaari, Pyry; Pistol, Mats Erik; Anttu, Nicklas

Published in:
Nanotechnology

DOI:
10.1088/0957-4484/27/43/435404

2016

Document Version:
Peer reviewed version (aka post-print)

Optimization of the short circuit current in an InP nanowire array solar cell through opto-electronic modeling

Yang Chen, Pyry Kivisaari, Mats-Erik Pistol and Nicklas Anttu

http://iopscience.iop.org/article/10.1088/0957-4484/27/43/435404/meta
Published in: Nanotechnology, 23 September 2016, 27, 43, 435404
The author would like to acknowledge the IOPscience publication group and Nanotechnology for the publication of this paper.
Doi: 10.1088/0957-4484/27/43/435404

Optimization of the short circuit current in an InP nanowire array solar cell through opto-electronic modeling

Yang Chen, Pyry Kivisaari, Mats-Erik Pistol, and Nicklas Anttu*

Division of Solid State Physics and NanoLund,

Lund University,

Box 118, 22100 Lund, Sweden

**nicklas.anttu@ftf.lth.se*

InP nanowire arrays with axial p-i-n junction are promising for next-generation photovoltaics with a demonstrated efficiency of 13.8%. However, the short-circuit current in such arrays has not matched their absorption performance. Here, we study through combined optical and electrical modeling how absorption of photons and separation of the resulting photogenerated electron-hole pairs define and limit the short-circuit current in the nanowires. We identify how photogenerated minority carriers in the top n segment (i.e., holes) diffuse to the ohmic top contact where they recombine without contributing to the short-circuit current. In our modeling, such contact recombination can lead to a drop of 60% in the short-circuit current. To hinder such hole diffusion, we include a gradient doping profile in the n segment to create a front surface barrier. This approach leads to a modest 5% increase in the short-circuit current, limited by Auger recombination with increasing doping. A more efficient approach is to switch the n segment material to the higher band gap GaP. Then, a much smaller amount of holes is photogenerated in the n segment, strongly limiting the amount of holes that can diffuse and disappear to the top contact. For a 500 nm long top segment, this GaP approach leads to a 50% higher short-circuit current than with an InP top segment. Such a long top segment could facilitate the fabrication and contacting of nanowire-array solar cells. These design schemes for managing minority carriers could open the door for higher performance in single- and multi-junction nanowire-based solar cells.

Keywords: InP, III-V semiconductor, nanowire array, solar cell, opto-electronic modeling

1. Introduction

Recently, III-V semiconductor nanowire-array based solar cells have shown increasing performance in efficiency. With a p-n junction in the axial direction, an efficiency of 15.3% was demonstrated for GaAs nanowires [1] and 13.8% for InP nanowires [20]. However, the measured short-circuit current in these solar cells was lower than expected from modeled absorption of photons in the nanowires [5, 10, 16, 21, 22, 25, 26]. One of the most probable reasons for this sub-optimal current is non-ideal collection of photogenerated carriers, and indeed, in the experiments on the InP nanowire array [5], it was found that photogenerated carriers in the top n segment showed a low probability to contribute to the short-circuit current. Later, it was argued that such a loss in the current could originate from the diffusion of photogenerated minority carriers into the ohmic top contact [1].

However, no rigorous modeling has been performed to elucidate the origin of this loss mechanism, or how to circumvent it. For example, the performance of nanowire array solar cells has been modeled rigorously [3] based on the Shockley-Queisser detailed balance between absorbed photons, emitted photons, and extracted current [17]. In that idealized modeling [3], in order to find the upper limit on the solar cell performance [23], neither non-radiative recombination nor possible diffusion of minority carriers into the ohmic contacts, i.e., the contact leakage, was included. In reality, varying non-radiative loss processes, such as Shockley-Read-Hall (SRH), surface and Auger recombination, as well as contact leakage can dominate the total recombination. Full opto-electronic modeling, including such non-radiative recombination, has been performed for both single-nanowire and nanowire-array solar cells [2, 24, 26, 28]. However, in those studies, collection of optically generated carriers and optimizing short-circuit current was not the focus of the analysis.

Here, we perform for an InP nanowire array (See Figure 1) a thorough analysis of (1) the absorption of incident photons and (2) the consequent splitting of the photogenerated electron-hole pair over the axial p-i-n junction. We study the probability to split the electron-hole pair as a function of photogeneration position. We confirm that the diffusion of photogenerated holes from the top n segment into the top contact is a major loss mechanism in the short-circuit current. We propose two different designs to hinder such diffusion of the minority carriers, that is, the holes in the n segment.

First, a gradient in the doping concentration in the top segment can be used for creating an electric field that deflects the photogenerated holes from reaching the top contact. However, the performance of this design is limited by increasing recombination losses with increasing carrier concentration due to the increased doping. In the second design, we use instead of InP the higher band gap GaP as the material for the top n segment. Due to the larger and indirect band gap, a much smaller amount of electron-hole pairs are generated in the top segment. Consequently, a much smaller amount of photogenerated holes can diffuse into the top contact. With this design, we can allow, thanks to the weaker photogeneration in the top segment, for a much larger top segment length without detrimental drop in the short-circuit current. The possibility to use a longer top segment could also facilitate the fabrication and contacting of nanowire-array solar cells. We believe that these design schemes for managing minority and majority carriers in nanowire photovoltaic devices open the door for higher performance in both single-junction and multi-junction nanowire-array based solar cells.

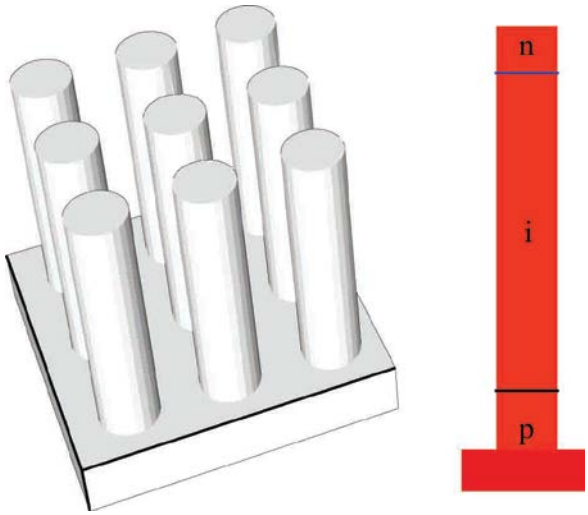

Figure 1. Schematic of an InP nanowire array with p-i-n junction.

2. Theoretical tools ─ Opto-electronics modeling

In the opto-electronics modeling of the short-circuit current, we solve for the absorption of incident photons and the consecutive separation and transport of the resulting electrons and holes. The optical response of the nanowire array is solved for with the Maxwell equations, and the electron-hole transport in the nanowires is solved for with the drift-diffusion formalism. We use the finite element method for this numerical analysis.

2.1 Optics modeling and optical generation function G(r)

We solve for the diffraction of light in the nanowire array with the Maxwell equations [4, 27] . In this modeling, we include the three-dimensional geometry of the nanowire array. The optical response of the constituent materials is described by their complex-valued refractive index, and we use tabulated values from [14] for InP and GaP, respectively. Note that we neglect for simplicity possible variation in the refractive index due to doping in the n and the p segments. Such effects are expected to cause only minor impact on the absorption for the doping concentrations considered in this study.

We solve for normally incident light, that is, for light incident parallel to the axis of the nanowires, and we use periodic boundary conditions with one nanowire per unit cell. As a result, we obtain the electric field **E**(**r**) throughout the system. From this electric field, we can calculate the local absorption of incident photons in the nanowires and the substrate, which is proportional to $\mathrm{Re}(n(\mathbf{r}))\mathrm{Im}(n(\mathbf{r}))|\mathbf{E}(\mathbf{r})|^2$ [21]. For a given incident intensity spectrum $I(\lambda)$ we can then calculate $G(\mathbf{r})$, the number of electron-hole pairs photogenerated per unit volume per unit time. This $G(\mathbf{r})$ enters the drift-diffusion modeling for the electron-hole transport [Eq. (1)]. For the calculation of $G(\mathbf{r})$, we use circular polarized light and an incident intensity given by the AM1.5D solar spectrum (ASTM G173-03) with total input power of 900 W/m^2.

2.2 Drift-diffusion modeling

We solve the electron-hole transport with the drift-diffusion formalism (See, e.g., Ref. [12]):

$$\begin{aligned} \nabla \cdot (-\varepsilon \nabla \varphi) &= q(p - n + N_d - N_a) \\ \nabla \cdot J_n = \nabla \cdot (-q\mu_n n \nabla \varphi_n) &= q(R - G) \\ \nabla \cdot J_p = \nabla \cdot (-q\mu_p p \nabla \varphi_p) &= -q(R - G). \end{aligned} \tag{1}$$

Here, ε is the (static) dielectric constant, q is the elementary charge, $\mu_{n/p}$ is the electron/hole mobility, $n(\mathbf{r})/p(\mathbf{r})$ is the electron/hole concentration, $\varphi(\mathbf{r})$ /$\varphi_n(\mathbf{r})$ /$\varphi_p(\mathbf{r})$ is the electrostatic potential/electron quasi-Fermi potential/hole quasi-Fermi potential, $N_{d/a}(\mathbf{r})$ is the density of ionized donors/acceptors, $R(\mathbf{r})$ is the net recombination rate and $G(\mathbf{r})$ is the above defined optical generation rate. Due to fast relaxation of optically generated carriers to quasi-equilibrium, the drift-diffusion model is sufficient for the purpose of this work. For R in the bulk of the nanowire, we use:

$$R = R_{SRH} + R_{rad} + R_{Aug} = \left(\frac{A}{n+p+2n_i} + B + C(n+p)\right)(np - n_i^2) \tag{2}$$

where $A/B/C$ is the recombination coefficient of SRH/radiative/Auger recombination, and n_i is the intrinsic carrier concentration [11, 12]. Here, we assume that the electron and hole densities are equal to n_i in the case where the Fermi level coincides with the trap level

responsible for SRH recombination, and we assume equal SRH lifetime for electrons and holes [18]. Regarding the Auger recombination rate, the same coefficient C is assumed for electron and holes. Since including wave-optical effects in light emission is very challenging and as we only consider the short-circuit current, we neglect radiative recombination in this study. That is, we use $B = 0$ in Eq. (2), however, see Supplementary data Section S1 for a discussion of possible effects from radiative recombination. The surface recombination, at the surface of the nanowire, is included through the term:

$$R_{surface} = \frac{V_{sr}}{n+p+2n_i}(np - n_i^2) \tag{3}$$

where V_{sr} is the surface recombination velocity [7].

In the drift-diffusion equations, the carrier concentrations n and p are calculated by:

$$n = N_c F_{\frac{1}{2}}\left(\frac{E_{F_0} - \varphi_n - E_c}{k_b T}\right)$$

$$p = N_v F_{\frac{1}{2}}\left(\frac{E_v - E_{F_0} + \varphi_p}{k_b T}\right) \tag{4}$$

$$N_{c/v} = 2\left(\frac{m^*_{e/v} k_b T}{2\pi\hbar^2}\right)^{\frac{3}{2}}$$

where k_b is Boltzmann constant, $m_{e/h}^*$ are effective mass of electrons and holes, $\hbar$ is reduced Planck constant, and E_{F0} is the Fermi level at zero bias voltage and zero optical generation:

$$E_{F_0} = E_{cn} + \left(\frac{k_b T}{q}\right) F_{\frac{1}{2}}^{-1}\left(\frac{N_{dn}}{N_c}\right) \tag{5}$$

where N_{dn} is the ionized donor density which equals the n doping level and E_{cn} is the conduction band edge at the n-type contact.

In the Equations (4) and (5), the functions $F_{1/2}$ and $F_{1/2}^{-1}$ are, respectively, the ½ order Fermi integral and its inverse function:

$$F_{\frac{1}{2}}(\eta) = \frac{2}{\sqrt{\pi}} \int_0^{\infty} \frac{x^{1/2}}{1+\exp(x-\eta)} dx. \quad (6)$$

In addition, the band edges are calculated as

$$E_v = \Delta VBO(r) - \varphi \quad (7)$$

$$E_c = E_g(r) + \Delta VBO(r) - \varphi \quad (8)$$

where $\Delta VBO(r)=VBO(r)-VBO_{InP}$ with VBO_{InP} the value for InP.

The specific values for the parameters used in the drift-diffusion modeling are listed in Table 1. Note that for simplicity in the modeling, we do not include doping induced band gap narrowing, or strain induced band offset in lattice mismatched heterostructures like the GaP/InP system in Section 7. Strain effects are important only close to the interface between InP and GaP, and the strain relaxes away from the interface. For the length of the GaP segment we use in Section 7, the strain is negligible at the top of the GaP segment.

Regarding the geometry used in this drift-diffusion modeling, we consider a single nanowire on top of a substrate. Note however that the $G(\mathbf{r})$ is calculated for the nanowire array. We place an ohmic contact at the top of the nanowire. The ohmic boundary condition at short circuit current is defined as:

$$[\varphi, \varphi_n, \varphi_p] = \begin{matrix} [0,0,0] & (n\ contact) \\ [-V_0, 0,0] & (p\ contact) \end{matrix} \quad (7)$$

where V_0 is

$$V_0 = E_g + VBO_p - VBO_n + \left(\frac{k_b T}{q}\right) F_{\frac{1}{2}}^{-1}\left(\frac{N_d}{N_c}\right) + \left(\frac{k_b T}{q}\right) F_{\frac{1}{2}}^{-1}\left(\frac{N_a}{N_v}\right) \quad (8)$$

$N_{a/d}$ is the p/n doping level at p/n contact, p_{VBO}/n_{VBO} is the valence band offset at p/n contact.

In the drift-diffusion modeling, the substrate has a lateral size equal to the unit cell size of the array and a depth of 300 nm. We placed an ohmic contact also at the bottom of the substrate and ascertained that the thickness of this substrate did not affect the resulting short-circuit current. Unless otherwise stated, we use a 100 nm long n segment and a 300 nm long p segment in the modeling, and both segments have an ionized doping density of 10^{18} cm^{-3}.

Parameters	InP	GaP
Dielectric constant (ε)	$12.5\varepsilon_0$	$11.1\varepsilon_0$
Surface recombination velocity (V_{sr})	200 cm/s	2×10^5 cm/s
Shockley-Read-Hall recombination coefficient (A)	10^7 s^{-1}	10^7 s^{-1}
Auger recombination coefficient (C)	9×10^{-31} cm^6/s	10^{-30} cm^6/s
Electron mobility (μ_n)	5400 $cm^2V^{-1}s^{-1}$	250 $cm^2V^{-1}s^{-1}$
Hole mobility (μ_p)	250 $cm^2V^{-1}s^{-1}$	150 $cm^2V^{-1}s^{-1}$
Bandgap	1.34 eV	2.26 eV
Valence band offset (VBO)	-1.27 eV	-0.94 eV

Table 1. The parameters used in the drift-diffusion modeling [13, 19], unless explicitly stated otherwise in direct connection to the presented results.

2.3 Spatially resolved internal quantum efficiency (SIQE)

For more detailed analysis of the charge separation mechanism within the nanowires, we used the spatially resolved internal quantum efficiency (SIQE). The SIQE is given by the spatially resolved probability $S(\mathbf{r})$ of an electron hole pair, injected at **r,** to contribute an elementary charge to the short-circuit current at zero bias voltage. Practically, we calculate $S(\mathbf{r})$ by using a generation rate density of $G_{SIQE} = 10^{28}$ $m^{-3}s^{-1}$ in a cubic box of volume V_{SIQE} with 10 nm side length, centered at r (we ascertained that the resulting SIQE did not vary noticeably with varying G_{SIQE} around this value.). That is, $V_{SIQE} = (10\text{ nm})^3$. Next, we calculate the short-circuit current $J_{sc,SIQE}$ that results from this injection using drift diffusion equations. Finally,

we obtain the SIQE as: $S(\mathbf{r}) = (1/q)\, I_{sc,SIQE} / (G_{SIQE} V_{SIQE})$. Note that a similar SIQE is used in Ref. [6] for the analysis of silicon nanowire photovoltaic devices.

3. Results and discussion — Factors limiting the short-circuit current from $J_{sc,max}$ = 31 mA/cm^2

From wave-optics, the absorption performance of the nanowire array depends on the nanowire diameter, the nanowire length, and the array pitch [3]. When considering the absorption of sun light, we typically turn to look at the short-circuit current J_{sc}. This current results from the absorption of photons and the consecutive separation of the photogenerated electrons and holes over the p-i-n junction. For the 900 W/m^2 direct and circumsolar AM1.5D solar spectrum, we obtain for InP with band gap E_g = 1.34 eV an upper limit of $J_{sc,max}$ = 31 mA/cm^2 by assuming that each incident photon with energy $E_{ph} > E_g$ is absorbed, and that each photogenerated electron hole pair contributes to the short-circuit current. Below, we consider the two effects that decrease J_{sc} from $J_{sc,max}$ — (1) Less than 100% absorption and (2) less than 100% probability to separate photogenerated charges over the p-i-n junction.

4. Results and discussion — Geometry dependence of short-circuit current

For nanowire arrays, the short-circuit current shows diameter dependent peaks [3] due to diameter-dependent absorption resonances in the nanowires. The diameter that optimizes the absorption depends on the band gap E_g of the nanowire material. For InP with E_g = 1.34 eV, the smallest diameter that optimizes the absorption performance is D = 180 nm. We fix D = 180 nm throughout this study, and we choose a nanowire length of L = 1400 nm to match experiments [21].

In Figure 2(a), J_{sc} is plotted as a function of the remaining free parameter, the pitch of the square array. In the drift-diffusion modeling (solid line in Figure 2(a)), we find a maximum value of 25.8 mA/cm^2 when the pitch is 330 nm. Also, we find J_{sc} = 24.2 mA/cm^2 for the pitch P = 470 nm, which has been used in previous experiments for InP nanowire arrays [21].

Both these short-circuit values are lower than the upper limit $J_{sc,opt}$ from absorption modeling (dashed line in Figure 2(a)), which predicts an upper limit of $J_{sc,opt}$ = 28 mA/cm^2 for J_{sc} assuming 100% contribution from all photogenerated carriers to the current. In contrast, the drift-diffusion modeling includes loss mechanisms that lead to a less than 100 % probability for splitting photogenerated electron-hole pairs over the p-i-n junction.

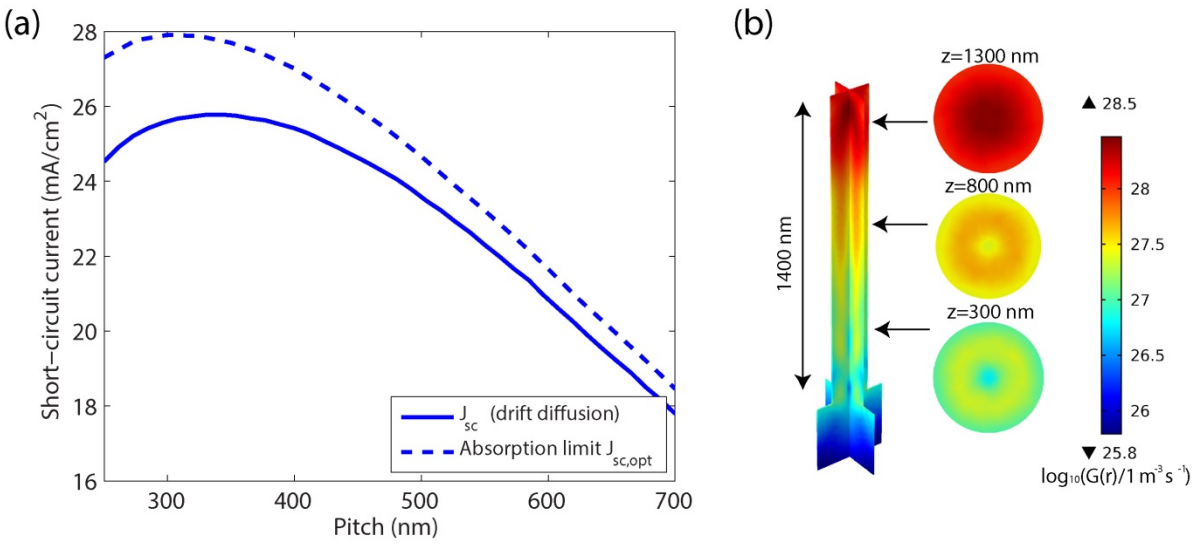

Figure 2. (a) Short circuit current as a function of nanowire array pitch. Here, we show the absorption limited $J_{sc,opt}$ (dashed line) as well as the J_{sc} from the drift-diffusion modeling (solid line). Note that for $J_{sc,opt}$ we assume a 100% probability for each photogenerated electron-hole pair to contribute to the short-circuit current. In contrast, in the drift-diffusion modeling we include varying recombination mechanisms that can decrease this probability. The nanowires are 1400 nm long with a 100 nm long n-doped top segment and a 300 nm long p-doped bottom segment. The ionized doping density is 1×10^{18} cm^{-3} for both the n and the p segment. (b) Optical generation rate $G(\mathbf{r})$ in one nanowire of the array in Figure 1.

To better understand the absorption properties of the nanowires, we turn to study the spatial distribution of the optical generation rate in the nanowire (Figure 2(b)). We find a very strong dependence of the generation as a function of the position along the axis of the nanowire. For example, 85% of the generation occurs in the top half of the nanowire. Also, the maximum generation rate in the nanowire is two orders of magnitude larger than in the substrate. This strong generation in the top part of the nanowires indicates that it is very important to maximize the probability to extract photogenerated carriers from this segment. Thus, in the

next subsection we investigate how the design of the p, i, and n segment affects this extraction probability.

5. Results and discussion — Doping segment length dependence

To investigate the possible effect of the design of the p, i, and n segment on the short-circuit current, we varied the segment lengths for the above fixed nanowire length L = 1400 nm. In this way, the photogeneration inside the nanowire does not change. Thus, any variation in J_{sc} originates from variation in the efficiency of splitting electrons-hole pairs over the p-i-n junction.

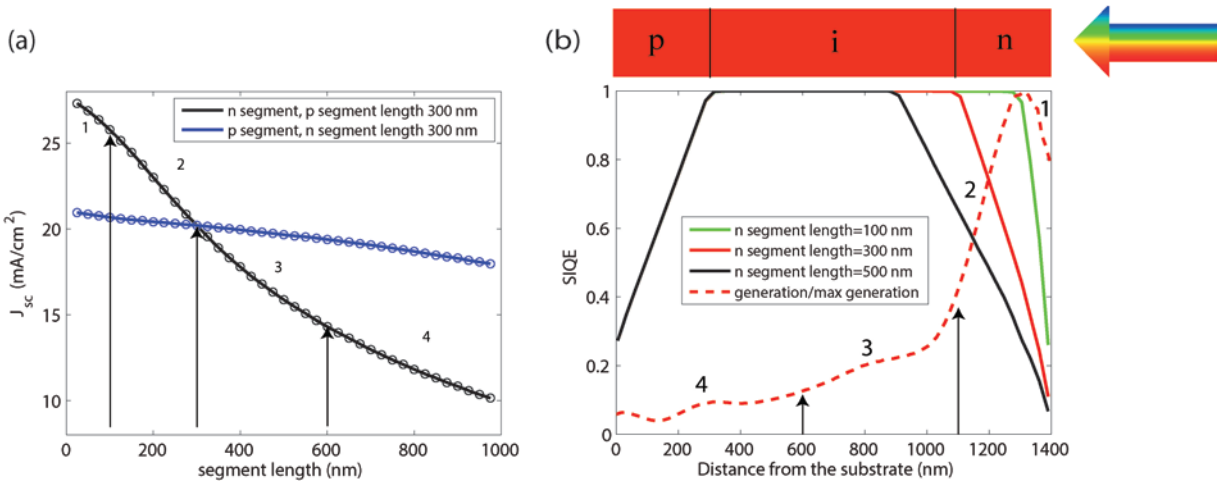

Figure 3. (a) J_{sc} as a function of n and p segment length for nanowires of diameter D = 180 nm and length L = 1400 nm placed in a square of pitch p = 330 nm on top of an InP substrate. For varying n (p) segment length, the p (n) segment length is kept constant at 300 nm. (b) Spatial internal quantum efficiency $S(\mathbf{r})$ in a nanowire of the array considered in (a), as a function of position along the axial direction. Here, we consider three different n segment lengths: 100, 300, and 500 nm (solid lines). We show also the normalized optical generation rate (dashed red line). Before the normalization, the generation rate was integrated over the cross section of the nanowire. A schematic of a nanowire with 300 nm long top n segment is placed at the top of this plot to aid the eye.

We varied the p segment length for a fixed n segment length of 300 nm (blue line in Figure 3(a)). Similarly, we varied the n segment length for a fixed p segment length of 300 nm (black line in Figure 3(a)). We find that J_{sc} is much more sensitive to a variation in the length of the top n segment than to a variation in the length of the bottom p segment. An increase of the

bottom segment length from 25 nm to 900 nm decreases J_{sc} just by 2.7 mA/cm^2, from 21.0 mA/cm^2 to 18.3 mA/cm^2. In contrast, J_{sc} decreases by 16.5 mA/cm^2, that is, by more than 60%, when the n segment length is increased by a similar amount. Note that a stronger dependence on the length of the top n segment length could be expected from the much stronger optical generation rate in the top part than in the bottom part of the nanowire (Figure 2(b)).

To obtain a better, quantitative, understanding of this strong dependence on the top n segment length, we studied the SIQE (solid lines in Figure 3(b) for varying length of the n segment). That is, we studied the spatially resolved probability $S(\mathbf{r})$ to split electron-hole pairs over the p-i-n junction (see section 2.3 for technical details). To aid in the analysis, we show also the optical generation rate in the nanowire (dashed red line in Figure 3(b)). First and foremost, we find a rapid decrease in the SIQE when moving in the n segment from the edge of the i segment toward the top contact. We find a similar drop in the p segment when moving down, away from the edge of the i segment. In contrast, the SIQE is close to 100% in the i segment. This drastically different behavior originates from the existence of an electric field in the i segment, which is lacking in the n and p segment. In the i segment, the electric field splits the electron and the hole rapidly and efficiently in opposite directions, leading to a high SIQE. In the n and p segment, the electron and the hole instead diffuse. For example, if a hole generated in the n-segment, which is the minority carrier, diffuses into the i segment, it will be swept toward the p side by the electric field and contribute to the current over the p-i-n junction. However, if the hole diffuses to the ohmic top contact, it contributes to current leakage and recombines in the contact. The probability for the hole to diffuse from the n segment into the i segment depends on the distance to the i segment and the distance to the ohmic top contact. Therefore, the SIQE decreases from close to 100% to close to 0 when the photogeneration position shifts from the edge of the i segment to the edge of the ohmic

contact. Note that a similar behavior/drop has been recently observed in electron-beam induced current measurements of individual, as-grown nanowires [1].

The number of holes that are photogenerated in the top n segment increases with increasing n segment length. Hence, with increasing segment length, more holes are available for diffusion to the top contact, leading to an increasing drop in J_{sc} in Fig. 2(a). Furthermore, the optical generation rate is high in the topmost 300 nm of the nanowire (dashed red line in Figure 3(b)). Therefore, an increase of the n segment length from 25 nm to 300 nm causes a rapid drop in J_{sc} (marked by region 1 and region 2 in Figure 3(a)). When the n segment length is further increased from 300 to 1100 nm, the decrease in J_{sc} is slower (marked by region 3 and region 4 in Figure 3(a)) since the optical generation rate is lower here than in the topmost 300 nm.

Thus, a shorter n segment length leads to a higher J_{sc} by decreasing the number of holes that can diffuse into the ohmic top contact. Such an effect of increasing J_{sc} with decreasing top n segment length has been already reported in experiments [21], however without assigning it to the diffusion of minority carriers into the top contact. Nevertheless, in experiments a drastic decrease of the n segment length can become impractical due to problems in contacting nanowires with a short top segment [21]. Below, in order to maximize J_{sc}, we present two alternative designs for limiting the diffusion of holes into the top contact.

6. Results and discussion — Gradient doping to prevent holes from reaching the top contact

Here, in order to maximize J_{sc}, we discuss the potential of using a gradient in the doping profile in the n segment to prevent photogenerated holes from reaching the top contact. Note that such a doping scheme is often used at the bottom side of planar solar cells in order to reduce the diffusion, and consecutive loss, of minority carriers into the back contact [8].

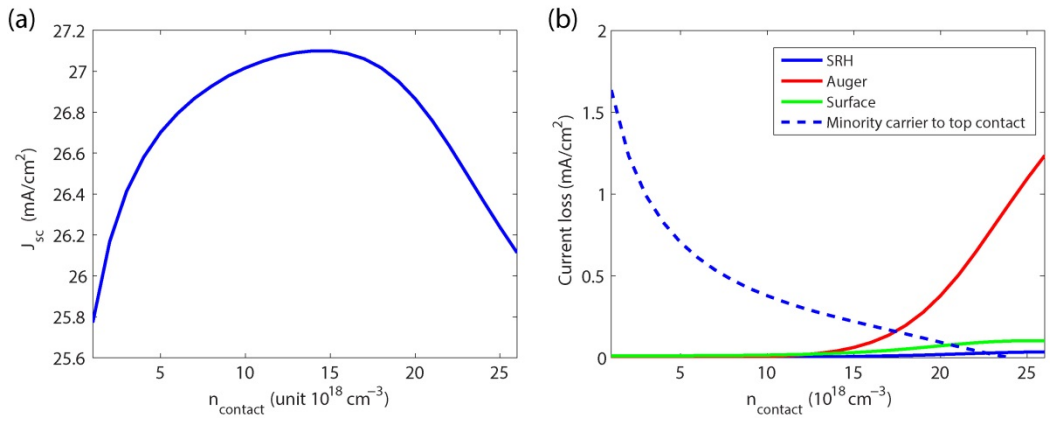

Figure 4. (a) J_{sc} as a function of $n_{contact}$, the doping concentration in the 100 nm long top n segment at the interface to the top contact. The doping concentration increases linearly to $n_{contact}$ from the value of 10^{18} cm^{-3} at the interface between the n and the i segment. (b) Minority current to the top contact and recombination, translated into equivalent current loss, as a function of $n_{contact}$.

We consider a linear increase in the doping concentration from 1×10^{18} cm^{-3} at the edge of the i segment to $n_{contact}$ at the edge to the ohmic contact. Here, we assume that the dopants are fully ionized. This gradient introduces an electric field in the n segment, which deflects the holes from reaching the top contact. In terms of the band diagram, this doping profile bends down the valence band edge toward the ohmic contact.

The J_{sc} is shown in Fig. 4(a) as a function of the doping density increase from the i-segment to the top contact. We find that J_{sc} increases initially with increasing gradient in the doping. When $n_{contact}$ increases from 1×10^{18} to 1.5×10^{19} cm^{-3}, J_{sc} increases from 25.8 mA/cm^2 to 27.1 mA/cm^2, that is, by 5%. To explain the curve shown in Fig. 4(a), Fig. 4(b) shows the different loss current mechanisms again as a function of the doping density increase. As expected, the minority carrier current, that is, the hole current, to the top contact decreases monotonously with increasing doping gradient, that is, with increasing $n_{contact}$ (dashed line in Figure 4 (b)). However, when $n_{contact} > 1.5\times10^{19}$ cm^{-3}, a further increase in $n_{contact}$ actually leads to a decrease in J_{sc} (Figure 4 (a)). This decrease originates from increasing recombination losses in the n segment due to the increasing carrier concentration with increasing doping.

Initially, when $1\times10^{18} < n_{contact} < 1\times10^{19}$ cm^{-3}, bulk SRH recombination is the dominant recombination mechanism in the case of the surface recombination velocity of 200 cm/s used here (see Supplementary data Section S2 for a discussion of the effect of increasing surface recombination velocity). In this case, the total recombination rate is several orders of magnitude lower than the corresponding minority carrier leakage to the top contact as seen in Fig. 4(b). Thus, for a low doping level, the major loss mechanism in J_{sc} is the diffusion of holes into the top contact.

However, with increasing $n_{contact}$, Auger recombination, which scales as carrier concentration to the third power, in contrast to SRH that scales as carrier concentration to the first power, sets in (solid line in Figure 4(b)). Auger recombination becomes significant when $n_{contact} = 10^{19}$ cm^{-3} and increases sharply for higher $n_{contact}$. For example, for $n_{contact} = 2\times10^{19}$ cm^{-3}, the Auger recombination amounts to 2% of the optical generation rate in the whole nanowire and starts to limit J_{sc} noticeably. Note that the large doping level in itself does not cause a net Auger recombination, but it induces a large Auger recombination velocity for the optically generated holes, which strongly reduces the benefit of gradient doping at very large doping levels.

Thus, by using a gradient doping profile in the top n segment, we can prevent the minority carriers, that is the holes, from reaching the top ohmic contact. With increasing doping gradient, we deflect the minority carriers more and more efficiently from reaching the contact. However, at the same time, we open up for Auger recombination of the photogenerated carriers, which decreases the overall current. Note that when such a gradient doping profile is used at the back side of a planar solar cell [8], we do not expect similar problems since the photogeneration rate is expected to be low on the bottom side of the solar cell.

7. Results and discussion — High band gap material for top n segment

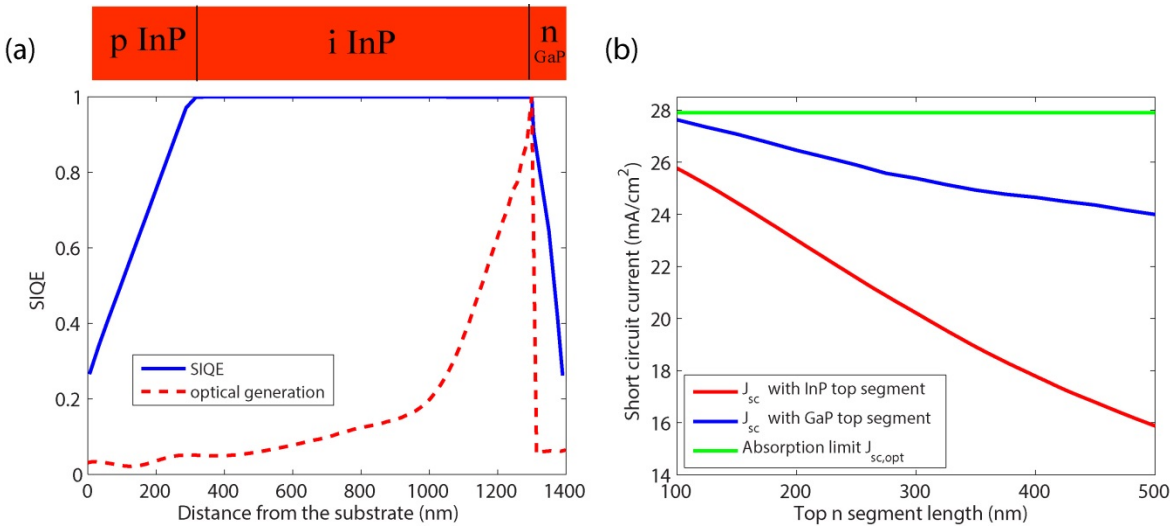

Figure 5. (a) SIQE, the spatially resolved internal quantum efficiency $S(\mathbf{r})$, and cross-section-integrated and normalized optical generation rate $G(\mathbf{r})$ in an InP nanowire of the array. The nanowires are of 180 nm in diameter and 1400 nm in length, and they have a 100 nm long GaP top n segment on top of an intrinsic InP segment, which is in turn on top of a 300 nm long InP bottom segment. The nanowires are placed in a square array of 330 nm in pitch on top of an InP substrate (b) Dependence of the J_{sc} on the n segment length for the nanowire array geometry in (a). Here, the nanowires have either a GaP top segment (blue solid line) or an InP top segment (red solid line). For comparison, we show for the case of an InP top segment the absorption limited short-circuit current $J_{sc,opt}$ (dashed line) where we assume that each photogenerated electron-hole pair contributes to the current.

To avoid the increased recombination losses introduced by the gradient doping profile above, we consider here a design with a semiconductor heterostructure. Our idea is to use for the top n segment a higher bandgap semiconductor in which only a small amount of holes is generated. In this way, only this small amount of holes can diffuse into the top contact. After consideration of both the band structure [15] and growth possibilities [9], we selected the indirect band gap GaP for the n segment. We keep the total length of the nanowire at the previously chosen L = 1400 nm. We have calculated the photogeneration rate for the case of a GaP top segment (dashed line in Figure 5 (a)), which should be compared to the case of an InP top segment in Figure 3(b). The optical generation rate in this GaP top n segment is only 9% of that in the InP i segment below, corresponding to 2.3 mA/cm^2. At the same time, we find in the i segment a close to 100 % charge separation, that is, SIQE ≈ 100 % (solid line in Figure

5(a)). This concentration of the photogeneration to this i segment with SIQE ≈ 100 % leads to a high J_{sc}, with values close to the absorption limited $J_{sc,opt}$.

Finally, when we compare the J_{sc} for varying n segment length (Figure 5(b)), we find much higher current levels with the GaP top segment than with the InP top segment. For a 100 nm long GaP segment, we reach a short circuit current of 27.6 mA/cm^2. This current level is very close to the above stated absorption limited $J_{sc,opt}$ = 27.9 mA/cm^2 in a 1400 nm long InP nanowire when all photogenerated carriers are extracted as current. Note that the overall absorption in the nanowire tends to decrease with increasing length of the GaP segment. For example, for a GaP segment of 500 nm in length, the drop in the overall absorption is equivalent to a photocurrent of 1.7 mA/cm^2 (see Supplementary data Section S3).

When the GaP segment length is increased from 100 nm to 500 nm, the current goes down from 27.6 to 24 mA/cm^2. In contrast, a similar increase of the n segment length when using InP for the top segment causes a much larger drop, from 25.7 to 15.9 mA/cm^2. Thus, for the 500 nm long top segment, the use of GaP gives a 50% higher short-circuit current. In this way, with the GaP top segment, we can allow for a relatively long top segment without losing current detrimentally.

8. Conclusion

We analyzed through modeling the short-circuit current in an InP nanowire array solar cell with a p-i-n junction in each nanowire. We assumed an ohmic contact on top of the top n segment, as is conventionally done in the fabrication of nanowire array solar cells. In such a structure, the photogenerated minority carriers in the n segment, that is, the holes, can diffuse readily to the close lying top contact. If a photogenerated hole indeed diffuses to the top contact, it recombines without contributing to the short-circuit current. If the hole instead manages to diffuse into the i segment, it is swept by the built in electric field to the p side,

which leads to a charge separation over the p-i-n junction and consecutively to a contribution to the short-circuit current.

By reducing the length of the top n segment, we reduce the number of photogenerated holes in this top segment. Therefore, we limit the number of photogenerated holes that are lost due to diffusion to the top contact, and the short-circuit current increases. However, a drastic decrease of the top segment length can lead to issues in the contact fabrication. A planarized contacting scheme is typically used for the top contact. Due to the standard deviation in both the nanowire length and the contact layer planarization, also a part of the side wall of the top segment is typically contacted, and the extent of this sidewall contacting varies from nanowire to nanowire. With a short top segment, it becomes impractical to contact each nanowire without forming a contact to the i segment in some nanowires. Therefore, we proposed two alternative designs to reduce the hole diffusion to the top contact.

In the first design, we increased the doping concentration in the n segment toward the top contact. Such gradient in the doping profile leads to an electric field in the n segment which hinders the holes from reaching the top contact. However, we found that the performance gain with this approach is limited by the increasing recombination losses due to the increasing carrier concentration with increasing doping.

In the second design, we replaced the InP in the n segment by the higher band gap GaP. Due to the larger indirect band gap of GaP, the number of photogenerated holes decreases dramatically in the top segment. Therefore, a much lower number of holes can diffuse from the top segment to the top contact. With this approach, we found that a considerably larger top segment length could be allowed for, without detrimental loss in the short-circuit current. At the same time, with such a longer top segment, we expect that we can allow for a larger

standard deviation in both the nanowire length and height/thickness of planarized contact layers.

In principle, this design with a high band gap top segment could be applied also to a tandem cell with GaInP/InP nanowires on top of a Si substrate cell, as well as to GaInP(GaAsP)/InP or GaInP(GaAsP)/GaAs nanowire tandem solar cell.

Acknowledgments

This work was performed within NanoLund and received funding from the People Programme (Marie Curie Actions) of the European Union's Seventh Framework Programme (FP7-People-2013-ITN) under REA grant agreement No 608153, PhD4Energy, and the European Union’s Horizon 2020 research and innovation programme under grant agreement No 641023, NanoTandem. This article reflects only the author's view and the Funding Agency is not responsible for any use that may be made of the information it contains. Kivisaari wants to express his gratitude to the Nokia Foundation and the Finnish Cultural Foundation for financial support.

Associated content

Supplementary data

The Supplementary material contains discussion of radiative and surface recombination in InP nanowires, and additional data on optical absorption in InP/GaP heterostructures. This material is available free of charge via the Internet at http://ioppublishing.org.

References

[1] Åberg I, Vescovi G, Asoli D, Naseem U, Gilboy J P, Sundvall C, Dahlgren A, Svensson K E, Anttu N, Björk M T and Samuelson L 2016 A GaAs Nanowire Array Solar Cell With 15.3% Efficiency at 1 Sun *IEEE J. Photovolt.* **6** 185-90

[2] Anna H. Trojnar C E V, Ray R. LaPierre, Karin Hinzer, Jacob J. Krich Optimizations of GaAs Nanowire Solar Cells *arXiv:1605.04410*

[3] Anttu N 2015 Shockley-Queisser Detailed Balance Efficiency Limit for Nanowire Solar Cells *ACS Photonics* **2** 446-53
[4] Anttu N, Lehmann S, Storm K, Dick K A, Samuelson L, Wu P M and Pistol M E 2014 Crystal phase-dependent nanophotonic resonances in InAs nanowire arrays *Nano Lett.* **14** 5650-5
[5] Anttu N and Xu H Q 2013 Efficient light management in vertical nanowire arrays for photovoltaics *Opt. Express* **21** A558-A75
[6] Christesen J D, Zhang X, Pinion C W, Celano T A, Flynn C J and Cahoon J F 2012 Design principles for photovoltaic devices based on Si nanowires with axial or radial p-n junctions *Nano Lett.* **12** 6024-9
[7] Darling R B 1991 Defect-state occupation, Fermi-level pinning, and illumination effects on free semiconductor surfaces *Phys. Rev. B* **43** 4071-83
[8] Demtsu S H and Sites J R 2006 Effect of back-contact barrier on thin-film CdTe solar cells *Thin Solid Films* **510** 320-4
[9] Dick K A, Kodambaka S, Reuter M C, Deppert K, Samuelson L, Seifert W, Wallenberg L R and Ross F M 2007 The morphology of axial and branched nanowire heterostructures *Nano Lett.* **7** 1817-22
[10] Foldyna M, Yu L W, O'Donnell B and Cabarrocas P R I 2011 Optical absorption in vertical silicon nanowires for solar cell applications *Proc Spie* **8111** 811110
[11] Heikkiia O, Oksanen J and Tulkki J 2009 Ultimate limit and temperature dependency of light-emitting diode efficiency *J. Appl. Phys.* **105** 093119
[12] Kivisaari P, Oksanen J and Tulkki J 2012 Effects of lateral current injection in GaN multi-quantum well light-emitting diodes *J. Appl. Phys.* **111** 103120
[13] Levinshtein M. R S a S M 1996 *Handbook Series on Semiconductor Parameters* vol 2: Ternary And Quaternary III-V Compounds World Scientific)
[14] Palik E D 1998 *Handbook of optical constants of solids* vol 3: Academic press)
[15] Pistol M E and Pryor C E 2009 Band structure of segmented semiconductor nanowires *Phys. Rev. B* **80** 035316
[16] Sandhu S, Yu Z and Fan S 2014 Detailed balance analysis and enhancement of open-circuit voltage in single-nanowire solar cells *Nano Lett.* **14** 1011-5
[17] Shockley W and Queisser H J 1961 Detailed balance limit of efficiency of p‐n junction solar cells *J. Appl. Phys.* **32** 510-9
[18] Shockley W and Read W T 1952 Statistics of the Recombinations of Holes and Electrons *Phys. Rev.* **87** 835-42
[19] Vurgaftman I, Meyer J and Ram-Mohan L 2001 Band parameters for III–V compound semiconductors and their alloys *J. Appl. Phys.* **89** 5815-75
[20] Wallentin J, Anttu N, Asoli D, Huffman M, Aberg I, Magnusson M H, Siefer G, Fuss-Kailuweit P, Dimroth F, Witzigmann B, Xu H Q, Samuelson L, Deppert K and Borgstrom M T 2013 InP nanowire array solar cells achieving 13.8% efficiency by exceeding the ray optics limit *Science* **339** 1057-60
[21] Wallentin J, Anttu N, Asoli D, Huffman M, Aberg I, Magnusson M H, Siefer G, Fuss-Kailuweit P, Dimroth F, Witzigmann B, Xu H Q, Samuelson L, Deppert K and Borgstrom M T 2013 InP nanowire array solar cells achieving 13.8% efficiency by exceeding the ray optics limit *Science* **339** 1057-60
[22] Wang B and Leu P W 2012 Tunable and selective resonant absorption in vertical nanowires *Opt. Lett.* **37** 3756-8
[23] Wang X F, Khan M R, Gray J L, Alam M A and Lundstrom M S 2013 Design of GaAs Solar Cells Operating Close to the Shockley-Queisser Limit *IEEE J. Photovolt.* **3** 737-44
[24] Wang X F, Khan M R, Lundstrom M and Bermel P 2014 Performance-limiting factors for GaAs-based single nanowire photovoltaics *Opt. Express* **22** A344-A58
[25] Wen L, Zhao Z, Li X, Shen Y, Guo H and Wang Y 2011 Theoretical analysis and modeling of light trapping in high efficicency GaAs nanowire array solar cells *Appl. Phys. Lett.* **99** 143116

[26] Witzigmann B, Yu S and Kupec J 2011 Analysis of semiconductor nanowire arrays for photovoltaics: IEEE) p 528-31
[27] Wu P M, Anttu N, Xu H Q, Samuelson L and Pistol M E 2012 Colorful InAs nanowire arrays: from strong to weak absorption with geometrical tuning *Nano Lett.* **12** 1990-5
[28] Yu S, Roemer F and Witzigmann B 2012 Analysis of surface recombination in nanowire array solar cells *JPE* **2** 028002